University of Nottingham

Research Project

Automated Optical Absorption System

Student Numbers:
14334056 & 14329769

October 28, 2023

Contents

Abstract

This paper investigates optical absorption within semiconductors and details and analyses an automated system to determine a semiconductor's energy band gap. Understanding the band structure and energy band gap of a semiconductor is crucial in determining its properties and how it can be commercially applied. With the prevalence of semiconductors on the rise across a plethora of industries, this is more pertinent now than ever. The system developed in this investigation seeks to be quick and easy to use whilst remaining accurate. The report explores three different optical absorption data analysis techniques which are all incorporated into the system. These include: a rapid method that calculates the band gap from raw transmission data of a semiconductor, the Tauc method which employs reputable Tauc analysis to determine the band gap and the sigmoid-Boltzmann method, hailed for its simplicity. For proof of concept, the system was used to calculate the energy band gap of a crystalline gallium arsenide (GaAs) wafer using all three analysis methods. This produced the band gaps 1.40($\pm$0.05)eV, 1.38($\pm$0.05)eV and 1.40($\pm$0.01)eV for the rapid, Tauc and sigmoid-Boltzmann methods respectively. This compares to the expected GaAs band gap of 1.42eV.

1 Introduction

1.1 History of Semiconductors

The history of semiconductor devices is short but rich. The concept of semiconductors has been around since Alessandro Volta, an Italian scientist made famous for his invention of the electric battery, who first mentioned the phenomena in 1792 [1].He noted that on account of their semiconducting nature, some materials do not conduct electricity and if they do, it soon vanishes [2]. However, it was Michael Faraday in 1833 who first documented the semiconducting effect, when he discovered the temperature dependence which silver sulphide has on its conductivity [3]. Both scientists lacked the conceptual understanding of the physics needed to establish the underlying reasons behind these phenomena. Since then, the semiconductor field has taken huge leaps to fill in the gaps in the knowledge with the basis for the first semiconductor devices established by Braun in 1874 [4]. However, his work was not appreciated until 1904 when the first primitive radio receiver (crystal detector) was developed. This was the first documented application of semiconductor devices [5]. Another key milestone was the first transistor comprised of semiconducting material, which was demonstrated by Bell laboratories in 1947 [6]. This invention allowed vacuum tubes to be replaced, which were far larger and used more power, proving semiconductors to be a far more elegant solution for use in electronics. Initially, the two elements silicon and germanium played a vital role in the development of semiconductor devices. However, it was silicon that in the end prevailed, in part due to it being operational at higher temperatures than its rivals. Silicon played such a crucial role in the semiconductor industry, that Silicon Valley was named after it [7].

The applications of semiconductors have come a long way, and are now synonymous with technology and everyday life, from uses in televisions to integrated circuit boards and solar cells. The effect which they have played on society cannot be underestimated and semiconductors have embedded themselves in many commercial sectors. As such, it comes as no shock that the semiconductor industry is worth $555 billion [8], with future predictions indicating that in 2028 it could be worth $ 893 billion [9].

1.2 Elementary Theory

The understanding of the physics behind semiconductors has progressed considerably from the time of Alessandro Volta and Faraday. It is now known that increasing the temperature of a semiconductor increases the concentration of charge carriers, both holes and electrons, which increases the electrical conductivity. The cause of this increase is the promotion of electrons from the valance band (a lower energy band) to the conduction band (a higher energy band). The difference between these two energy levels is called the band gap (E_g). The band gap is unique to the material and therefore varies. However, there is a trend; insulators have a large band gap, metals have little to no band gap and semiconductors have a band gap in between these two categories [10]. The band gap correlates directly to the electrical conductivity such that a smaller band gap enables the current to flow more easily. When energy (in the form of heat or light) is applied, this allows electrons to be promoted through the band gap, leading to increased electrical conductivity [11]. This band gap dictates the electrical and thermal properties of the material. Therefore knowing the band gap is key to understanding the properties of a specific semiconductor.

1.3 History of Band Gap Calculation

The determination of the band gap within semiconductors has been considered for some time, with the earliest papers dating back to 1952 [12]. Now a multitude of techniques can calculate a semiconductor's band gap. A typical undergraduate method of calculating the band gap is shown by Martil and Diaz [13]. This technique uses transmission measurements to calculate the absorption and hence calculate the band gap via Tauc plotting. This is the technique most similar to the one used in this experiment bar the addition of a lock-in amplifier to their experimental setup. Another simple technique is one in which the voltage is measured across the p-n junctions. This value is then used in conjunction with the equations $E_g(T) = E_g(0) - aT$ to approximate the band gap [14]. This however has the downside of having an innate temperature dependence as the current passing through the semiconductor causes the temperature to rise and vary the result. Experimental techniques have come a long way from the earliest papers and now complex machine learning models are being developed to determine the band structure of materials. One example of this would be an experiment conducted by Zhuo et al. [15], where a machine learning algorithm was developed to calculate the band gap of the material. This technique can accurately calculate the band gap based only on the composition of the material. Such a technique is incredibly versatile and represents the state of the art of current methods.

1.4 This Experiment

This experiment will introduce a novel automated method for calculating the band gap which differs from more typical methods. A range of automated methods are used in the experiment including a fast band gap calculation, the Tauc plotting method and the sigmoid-Boltzmann function method. Such techniques themselves are not novel but how they have been automated is. This experiment aimed to create automated systems which required little to no user inputs at all, such that the band gap calculation was automated. Another key aim was to make the system fast yet as accurate as possible. This is valuable when a multitude of samples' band gaps need calculating and longer methods would be more time-consuming.

2 Theory

2.1 Band structure

2.1.1 Banding of atomic orbitals

Optical effects arise from transitions between the bands and states in a semiconductor. The band structure is therefore critical to the optical properties of a semiconductor. There are many techniques which can accurately determine the band structure. However in a solid, atoms are closely packed resulting in electrons having a complex potential energy profile [10] . This is partially due to vibrations in the solid developing time dependant variations in the potential energy. Given these complexities, this investigation focuses on the more quantitative aspects of the theory.

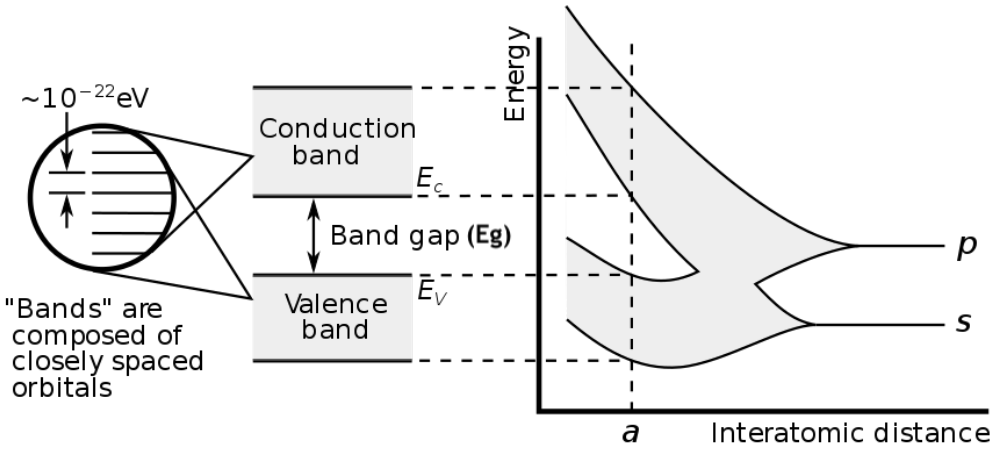

Figure 1: Energy banding of allowed levels as a function of the spacing between atoms

In free space, electrons have a continuous number of energy levels that can be occupied. However as a result of quantum mechanics, when confined to an atom, only a discrete set of energies are allowed. "As two similar atoms approach each other, the wave functions of the electrons begin to overlap. To satisfy Pauli's exclusion principle, the states of all spin-paired electrons acquire energies which are slightly different from their values in an isolated atom. It follows that if N atoms are packed within a range of interactions, $2N$ electrons of the same orbital can occupy $2N$ different states, forming a band of states instead of a discrete level as in the isolated atom" [16]. The distribution of the energy levels is strongly dependant on the interatomic distance. This is illustrated in Figure 1 which demonstrates a hypothetical assemblage of N (carbon) atoms. One can see the progression from having discrete s and p orbitals with the same energy, to when the atoms' electrons wave functions start to overlap causing the band to smear, forming a continuous energy band. At the distance denoted a (the atomic separation) two bands are formed. These are the valance and conduction bands, and as shown are separated by the band gap (E_g). As shown in Figure 1, there are no allowed states in the energy gap, therefore one would not expect to find an electron within that range of energies.

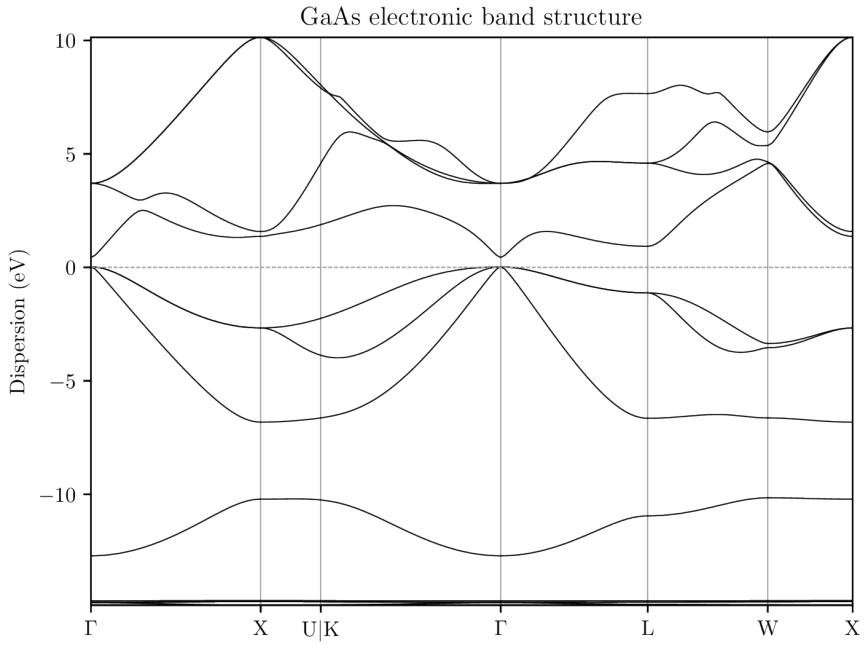

Figure 2: Illustrates the complex band structure of GaAs as a function of k space – computed AiiDA's PwBandsWorkChain

There are regions in which no electrons can reside. These regions correspond to energies which are forbidden in that particular material [17]. Figure 2 shows an example of a band structure of GaAs as a function of the wave vector k. The symbols Γ, L, X, W, K, represent critical points in the Brillouin zone. As shown the band structure is complex and has many forbidden energy bands, however, the most commonly discussed one and the focus of this experiment is the main band gap (E_g) which occurs at Γ in Figure 2. These forbidden regions are a direct result of there only being a particular set of energies which are solutions to the wave equation [11]. The bands of interest in the experiment are the two closest to minimal dispersion at the Γ point, being the valence and conduction bands. The valence band is the band in which the highest energy electrons reside within the orbital while still bound to the atom. The conduction band, in the case of semiconductors, is the band which contains electrons that have gained enough energy to be promoted from the valence band [18]. The relative positions of these bands and therefore the associated band gap is material dependent but there are three main categories in this spectrum: metals, semiconductors and insulators.

Metals have little to no band gap, insulators have a band gap in the region of > 3eV and semiconductors have a band gap in the range of 0.1 to 3 eV. Whilst semiconductors have a forbidden region between the conduction band and the valence band, it is small enough that a finite quantity of thermal or light energy is enough for an electron to bridge the gap between the bands. It should also be noted that semiconductors are flexible as their band gap can be manipulated. This can occur when an intrinsic semiconductor is doped with impurities making it either a n-type or a p-type. N-type semiconductors are doped with atoms which have an excess of electron donors. P-type semiconductors are doped with electron acceptors, with the Fermi levels shifting in accordance with the doping as shown in Figure 3.

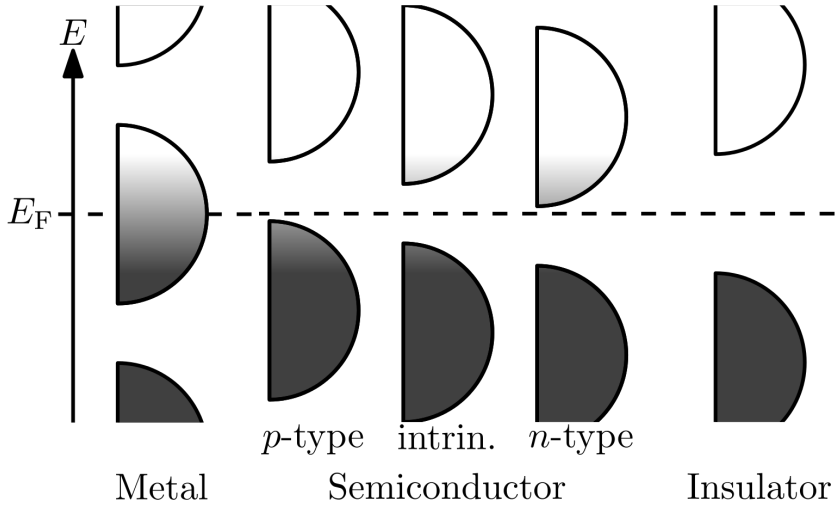

Figure 3: Illustrates the difference in band gap magnitude and positioning of the Fermi level for different types of material

2.1.2 Distribution in momentum space

As shown in Figure 1, there are definitive energy assignments for the allowed states. However, the allowed energy states are also distributed in momentum space. Energy and momentum are important, as both must be conserved within an optical transition. The kinetic energy of a free charge carrier is $E = \frac{1}{2}mv^2$ where m and v are its mass and velocity respectively. The momentum of the charge carrier, p, is given by $p = mv = \hbar k$ and $\hbar = \frac{h}{2\pi}$ where h is Plancks constant and k is the wave vector. Substituting p into the kinetic energy equation yields a classical and quantum mechanical relationship between kinetic energy and momentum:

$$E = \frac{p^2}{2m^*} = \frac{\hbar^2 k^2}{2m^*} \tag{1}$$

where the effective mass is given by m^*. Although the typical depiction of the energy varying will be along one dimension, the allowed energies vary in three, such that:

$$E = \frac{h^2 k^2}{2m^*}(n_x^2 + n_y^2 + n_z^2) \tag{2}$$

where n is the quantum number given in integers. While the energy varies in discrete steps, since the steps are small for the quantum number ($\approx 10^{-18}$ eV for a $1\mathrm{cm}^3$ crystal) , the energy appears quasi-continuum. The varying of energy along one dimension is given by the parabolic dependence which is illustrated in Figure 4. The states far away from the band edge are rarely occupied as the distribution function drops off exponentially. As such one may ignore the exact band structure of the material and focus solely on the band edges. In these regions, one can expand the energy dependence in Taylor series of second order in k around the conduction band minimum and the valence band maximum respectively [19]. This is known as the parabolic band approximation, shown in the following equation:

$$E \approx E_0 + \frac{(k-k_0)^2}{2}\frac{\partial^2 E}{\partial k^2}\bigg|_{\mathbf{k}=\mathbf{k_0}} \tag{3}$$

where E_0 and k_0 is the respective energy and wave vector about which the Taylor expansion is calculated. This type of curvature is indicative of the conduction band, that being the upward curvature. On the other hand, the valence band has a signature downward curvature. The significance of this is that, if the band were not fully filled, the electrons would accelerate in a direction opposite to that if they were in the conduction band as if they have negative mass. The top of the valance band is typically the reference level for the energy, and the bottom of the conduction band corresponds to the energy gap.

2.1.3 Band Gap Types

There are two basic band gap types: direct and indirect band gaps. In a direct band gap the valence band and the conduction bands valleys lie at $k = 0$ ($k_x = k_y = k_z = 0$). However, the minimum and maximum of these valleys need not be at the $k = 0$, as is the case in indirect semiconductors [16]. Such typical band gaps are illustrated in Figure 4.

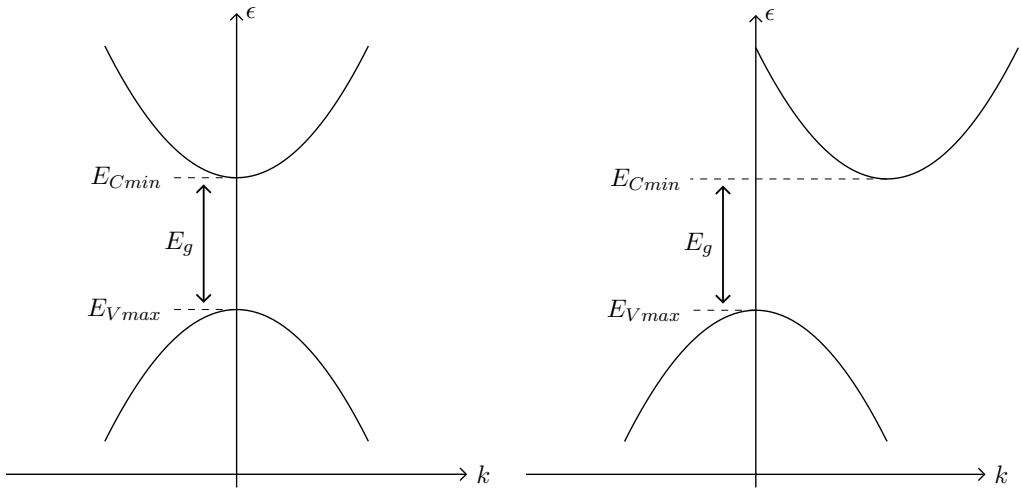

(a) Direct band gap **(b)** Indirect band gap

Figure 4: This figure illustrates the two main types of band gap transitions found in semiconductors

2.1.4 Density of States

The density of allowed states is uniform in momentum space. In three dimensions, such as in this experiment, the volume of k space between k and $k+dk$ is $4\pi k^2 dk$ which is approximately spherical. In addition the density of k states per unit volume is $\frac{2}{(2\pi)^3}$, which is found by identifying the periodic boundary conditions $\Psi\ e^{i\mathbf{kr}}$ (where Ψ is the wavefunction and **r** the position vector) and $k = \frac{2\pi}{L}n$ (where L is the length of the potential well). Therefore the number of k-states between k and $k + dk$ per unit volume is given by

$$D(k)dk = \frac{2}{(2\pi)^3}4\pi k^2\, dk \tag{4}$$

which becomes:

$$= \frac{k^2}{\pi^2} dk \tag{5}$$

$$\text{as } D(E)dE = D(k)\, dk \tag{6}$$

$$\therefore D(E) = \frac{\frac{k^2}{\pi^2}}{\frac{dE}{dk}} \tag{7}$$

Assuming a parabolic energy dispersion, which is accurate around the band edges.

$$E(k) = \frac{\hbar^2 k^2}{2m} \tag{8}$$

$$\therefore k = \sqrt{\frac{2mE}{\hbar^2}} \tag{9}$$

Differentiating Equation 8:

$$\frac{dE}{dk} = \frac{\hbar^2 k}{m} \tag{10}$$

$$\therefore D(E) = \frac{1}{2\pi^2\hbar^3}(2m^*)^{\frac{3}{2}} E^{\frac{1}{2}} \tag{11}$$

$$\therefore N(E)dE = \frac{1}{2\pi^2\hbar^3}(2m^*)^{\frac{3}{2}} E^{\frac{1}{2}}\, dE \tag{12}$$

2.1.5 Fermi-Dirac Distribution

Thus far the distribution of energy and momentum states have been dealt with. Now the occupancy of these states must be considered. The density of electrons is simply the product of the density of states and the Fermi Dirac function:

$$f(E) = \frac{1}{e^{\left(\frac{E-E_f}{k_B T}\right)} + 1} \tag{13}$$

where k_B is the Boltzmann constant, T is the absolute temperature and E_f is the Fermi energy. A graphical representation of this function can be seen in Figure 13, which shows the function in relation to the conduction and valence bands.

The Fermi-Dirac function simply provides the probability of a particular energy state being occupied at a given temperature. A feature of the Fermi-Dirac function is that with increasing temperature the probability that higher energy levels will be occupied increases. As shown in Figure 5, the Fermi-Dirac function can have values within the band gap. However, as noted before still no electrons occupy this region as the concentration is a product of the Fermi Dirac function and the density of states (which is zero in the forbidden region). At higher temperatures, the Fermi-Dirac function starts to have a probability in the conduction band, which leads to electrons residing in that region. This is in contrast to absolute zero where there are many states but the Fermi-Dirac function is zero leading to no electrons in the conduction band.

The Fermi level (E_f) is the highest energy level that can be occupied at absolute zero by an electron. At absolute zero, no electron has enough energy to be promoted above it.

The Fermi level is unique to each material and therefore lies in differing places. In an ideal semiconductor, the Fermi level lies centred in the middle of the band gap as shown in Figure 5. This however is not typically the case, as impurities within the semiconductor cause the Fermi level to skew either towards the conduction or valence band. This is shown in Figure 3 where n-type semiconductors' Fermi level moves towards the conduction band and the p-type towards the valence band. This signifies a change in the chemical potential of the semiconductor.

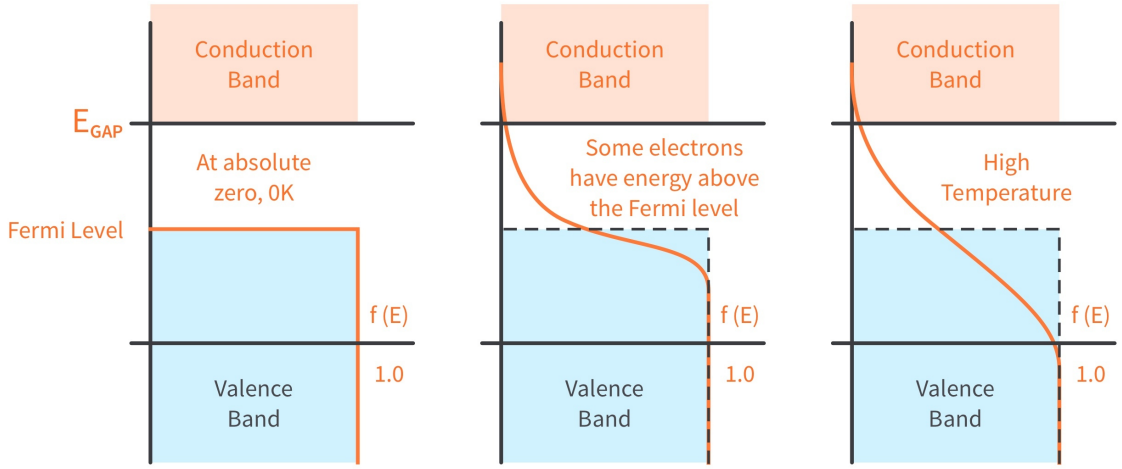

Figure 5: Demonstration of the effect of varying temperatures on the Fermi-Dirac distribution

2.2 Fundamental Absorption

2.2.1 The fundamentals

Absorption is typically expressed via the coefficient $\alpha(h\nu)$, which is simply defined as the relative rate of decrease in light intensity $L(h\nu)$ along its propagation path, x:

$$\alpha = \frac{1}{L(h\nu)} \frac{d[L(h\nu)]}{dx} \tag{14}$$

Fundamental absorption refers to band-to-band or exciton transitions. Fundamental absorption manifests itself via a rapid rise in absorption which is used to determine the semiconductor's band gap. These transitions are however subject to certain rules, which make estimating the band gap from the absorption edge complex even if other absorption processes are taken into effect.

Another key equation to realise is that of the momentum relating to photons. The equation is given by:

$$p = \frac{hc}{\lambda} \tag{15}$$

where λ is the wavelength and c is the speed of light. This equation is important as along with the energy, momentum has to be concerned. The wavelength of a photon is around three orders of magnitude greater than the spacing between the atoms, whereas the electron has the same magnitude [20]. Thus, the momentum of the photon is negligible in comparison to the electron,

following Equation 15. Therefore, absorption of solely a photon will not affect the position in k space of the electron, this is the case for direct transitions. If the electron's position in k space needs to be altered and the momentum change from the photon is insufficient, this change needs to be caused by either the emission or absorption of a phonon as illustrated in Figure 7.

It is well documented that by increasing the number of particles partaking in a mechanism, the probability of that process decreases accordingly. An example of an efficient mechanism is a direct band gap, which only involves two particles (a photon and an electron), for which the absorption coefficient is typically high: $\alpha \approx 10^4 - 10^5 \text{cm}^{-1}$ [21]. However, a mechanism such as an indirect band gap which utilises three particles has a lower absorption coefficient of around $\alpha \approx 10^3$.

2.2.2 Allowed Direct Transitions

The simplest mechanism for absorption occurs when an electron is promoted via the absorption of a photon. This causes the electron to be excited from the valence to the conduction band as shown in Figure 6. From the diagram it can be seen that the initial and final states of the electron can be linked by the following equation:

$$E_f = hv - |E_i| \tag{16}$$

where the initial and final states are given by E_i and E_f respectively and hv is the energy of the photon. For the electron to be promoted it must have sufficient energy. This threshold energy is equal to the band gap of the semiconductor (providing there are no impurities). It follows that there is a threshold for optical absorption, being that of the band gap, above which there is a near continuous range of possible transitions.

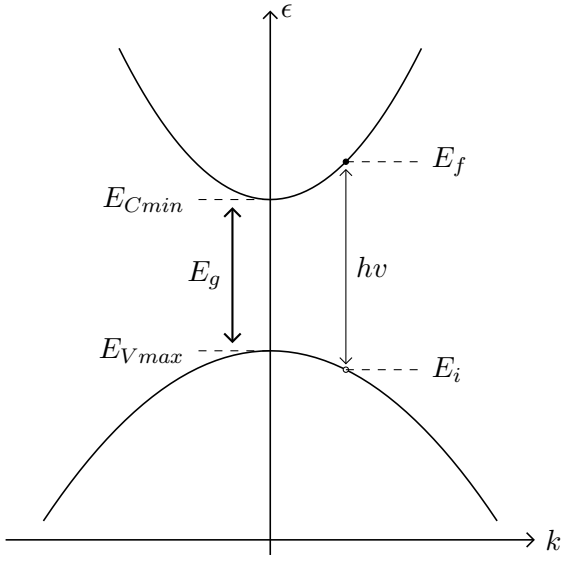

Figure 6: Direct band gap demonstrating an example transition

Following from Equations (1) and (16) two equations are found:

$$E_f - E_g = \frac{\hbar^2 k^2}{2m_e^*} \tag{17}$$

$$E_i = \frac{\hbar^2 k^2}{2m_h^*} \tag{18}$$

where m_e^* and m_h^* represent the effective mass of an electron and a hole respectively. Combining Equations (16), (17) and (18) yields

$$hv - E_g = \frac{\hbar^2 k^2}{2}\left[\frac{1}{m_e^*} + \frac{1}{m_h^*}\right] \tag{19}$$

$$= \frac{\hbar^2 k^2}{2}\left[\frac{1}{m_r^*}\right] \tag{20}$$

$$= \frac{\hbar^2 k^2}{2m_r^*} \tag{21}$$

in which m_r^* represent the reduced mass. Then Equation (21) is used to derive the density of directly associated states giving the following equation:

$$N(hv)d(hv) = \frac{(2m_r^*)^{\frac{3}{2}}}{2\pi^2\hbar^3}(hv - E_g)^{\frac{1}{2}}\, d(hv) \tag{22}$$

which resembles Equation 12. Therefore, by simplifying Equation 22 the absorption coefficient for direct allowed transition is:

$$\alpha(hv) = A^*(hv - E_g)^{\frac{1}{2}} \tag{23}$$

where the constant A^* is the factor:

$$A^* = \frac{(2m_r^*)^{\frac{3}{2}}}{2\pi^2\hbar^3} \tag{24}$$

Equation 23 demonstrates what should be observed regarding absorption with a direct band gap between parabolic bands, i.e the absorption rising with the square root of the energy of the photon.

2.2.3 Indirect Transitions between Indirect Valleys

In certain semiconductors, the valleys of the valence and conduction band do not lie in the same k space, such a band gap is called indirect. In such a transition the energy and the momentum of the electron need to be changed. Indirect transition cannot be conducted by a

photon alone, as its momentum is insufficient to change the electron's momentum sufficiently. Instead to conserve momentum, in addition to the photon a phonon is needed. A phonon is a quantum vibration of the lattice. Much like photons, despite there being a multitude of available phonons, only those with the correct energy and momentum value will be usable, each with a characteristic energy E_p. To complete this transition, the phonon can either be absorbed or emitted, both of which are demonstrated in Figure 7.

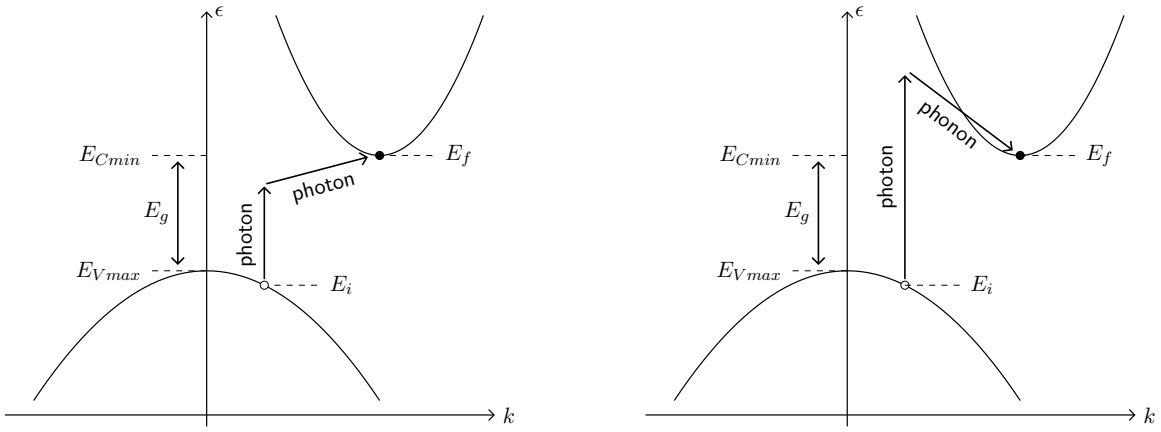

(a) Indirect band gap phonon absorption **(b)** Indirect band gap phonon emission

Figure 7: This figure illustrates the two different mechanisms that enable indirect band gap transitions

The two processes are given respectively by:

$$hv_e = E_f - E_i + E_p \tag{25}$$
$$hv_a = E_f - E_i - E_p \tag{26}$$

Similarly to direct band gaps, the density of states at an energy E is given by Equation 12. As such via substituting Equations 16 and 26 into Equation 12, the density of states at energy E_f is found to be:

$$N(E_f) = \frac{(2m_e^*)^{\frac{3}{2}}}{2\pi^2\hbar^3}(hv - E_g \pm E_p + E_i)^{\frac{1}{2}} \tag{27}$$

To find α it is paramount to realise that the absorption coefficient is proportional to the product of the density of states for the initial and final states, given by Equations 12 and 27 integrated over all states separated by $hv \pm E_p$. In addition it is also proportional to the probability of the phonons themselves interacting which in itself is a function. Neither the integration nor the derivation for the number of phonons which is given by Bose-Einstein statics will be given here but further calculations can be seen at [16]. After the integration and substitution of the said equation, the absorption coefficient for phonon absorption is given by:

$$\alpha_a(hv) = \frac{A(hv - E_g + E_p)^2}{e^{\frac{E_p}{kT}} - 1} \tag{28}$$

for the region $hv > E_g - E_p$. Similarly, the absorption coefficient for phonon emission is given by:

$$\alpha_a(hv) = \frac{A(hv - E_g - E_p)^2}{1 - e^{\frac{E_p}{kT}}} \tag{29}$$

for the region $hv > E_g + E_p$. As both of the transitions are possible in the region $hv > E_g + E_p$, the absorption coefficient is consequently a combination of both leading to the absorption coefficient:

$$\alpha(hv) = \alpha_e(hv) + \alpha_a hv \tag{30}$$

A graphical representation of the absorption coefficient is shown in Figure 8. For low energies ($hv > E_g - E_p$), it can be seen that a plot of $\alpha^{\frac{1}{2}}$ against energy will produce a straight line, the horizontal intercept being $E_g - E_p$. In addition, if $\alpha_e^{\frac{1}{2}}$ is plotted against energy, for high energies ($hv > E_g + E_p$), the straight line region yields a value for $E_g + E_p$. The value of α_e can simply be calculated by using Equation 30

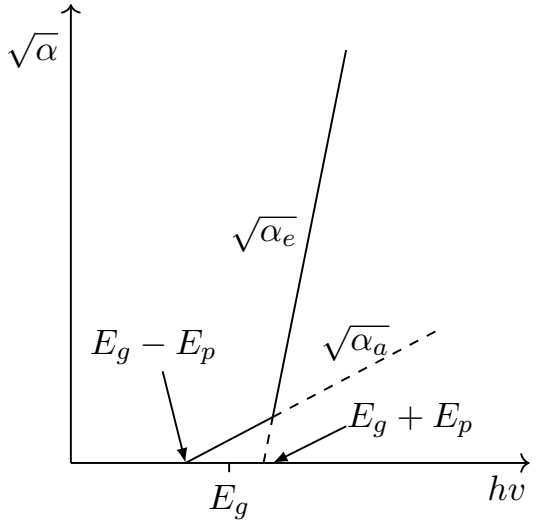

Figure 8: A theoretical representation of $\sqrt{\alpha}$ against energy, with the intercepts of importance being shown

2.2.4 Experimental Discrepancies

Equation (23) predicts no absorption below the band gap for a direct transition, and a steeply rising absorption edge afterwards. However ideal scenarios are contrary to what happens experimentally. As shown in Figure 9, in an experimental setting there is a ramping up of absorption and not a straight vertical line. This might be due to several factors but one of the main reasons is that the conduction and valence bands are not perfectly parabolic. Instead they have a "tail" which extends into the band gap region. In this region, the absorption coefficient denoted in Equation (23) is not adhered to. This band tailing is called Urbach's tail and the relationship in this region is given by Urbach's rule [22]:

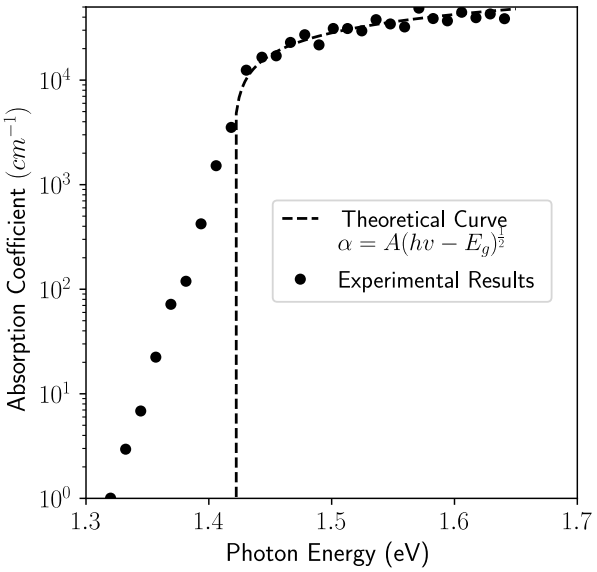

Figure 9: This Figure depicts the difference in the experimental and theoretical absorption spectra for a GaAs sample

$$\ln \alpha = \ln \alpha_0 + \frac{hv}{E_0} \tag{31}$$

where α_0 is a fitting parameter and E_0 is the Urbach energy. The effect the Urbach tail has on the band structure of a given semiconductor is shown in Figure 10, where energy states become available in the band gap region. This shows why absorption does not imminently jump from zero to full absorption but instead gradually increases, as photon energies approach the band edge.

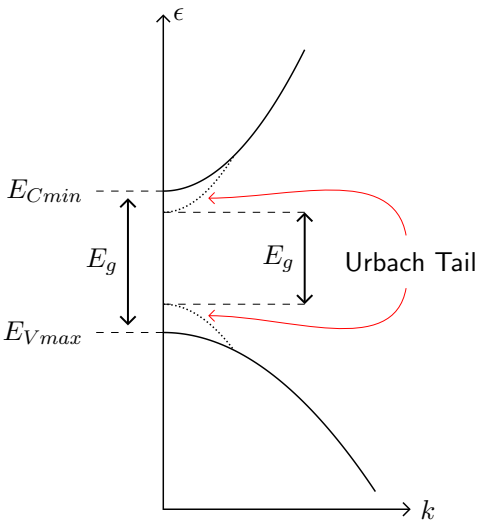

Figure 10: This Figure depicts how the presence of the Urbach tail diminishes the energy band gap of a semiconductor

2.2.5 Experimental Implementation

A key aspect regarding the optics of a semiconductor which has not been discussed is the transmission coefficient T. Experimentally, the transmission coefficient is useful as it is commonly used to calculate the value for the absorption coefficient. The transmission coefficient shown in Equation 32 is defined as the ratio of the incident and transmitted light intensity. In practical terms this is typically measured as a current or voltage.

$$T \equiv \frac{I}{I_0} \tag{32}$$

The relation between the transmission coefficient and absorption coefficient is not trivial, as factors such as internal reflections and changing refractive index need to be accounted for. In a material with thickness t, reflectivity R and an absorption coefficient of α, the radiation traversing the first interface is $(1-R)I_0$ and the radiation reaching the second is $(1-R)I_0e^{-\alpha t}$. After multiple internal reflections, it can be shown that only the fraction $(1-R)^2I_0e^{-\alpha t}$ emerges. As such the overall transmission is given by:

$$T = \frac{(1-R)^2I_0e^{-\alpha t}}{1-R^2e^{-2\alpha t}} \tag{33}$$

and with some algebraic manipulation, the formula can be rearranged for α such that:

$$\alpha = \frac{1}{t}\ln\left(\frac{((1-R)^4+4T^2R^2)^{0.5}-(1-R)^2}{2T^2R^2}\right) \tag{34}$$

The values of R and T, can be found experimentally. Theory behind the absorption coefficients form the foundations of the Tauc plotting used in this report.

3 Experimental method

The experimental setup used in the automated optical absorption system can be seen in Figure (11). Monochromatic light from the Bentham M300 monochromator was shone onto the semiconducting sample mounted to the lab top, which was placed directly in front of a ThorLabs DET10A silicon (Si) photodetector. A silicon detector was chosen as it gave the most appropriate wavelength sensitivity range, 300-1100 nm, for the selected test specimen. The photodetector was connected to a 102 Ω resistor which was connected to a multimeter. The current produced from a photodetector can be small, especially when little light is incident upon its photosensitive eye. By placing a large resistor across the detector's output, the voltage is easier to read for the voltmeter. The multimeter and the monochromator were connected to the computer via a DAQ card. While under experimental conditions, the system was operated in darkness to ensure the only light incident on the photodetector was from the monochromator.

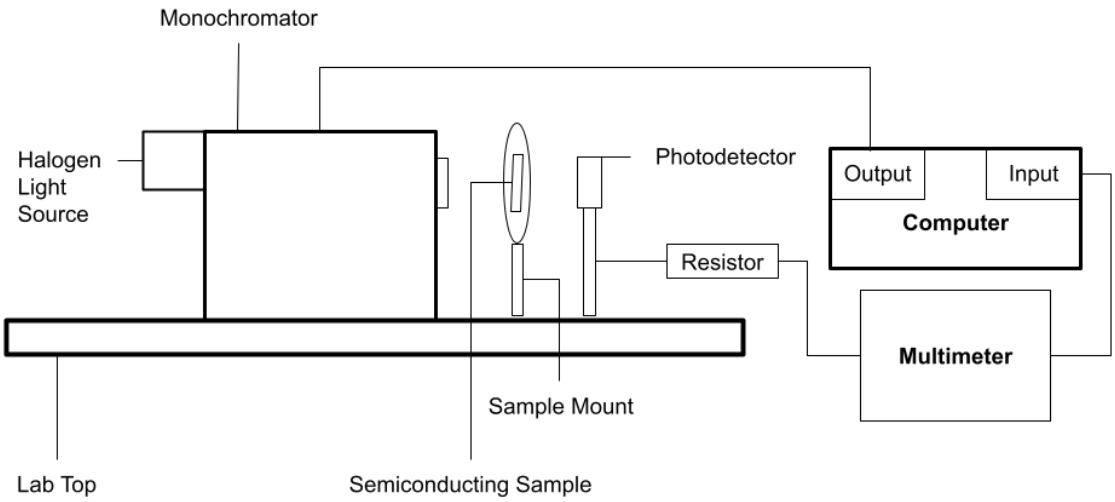

Figure 11: This Figure presents the equipment that comprises the automated optical absorption system

3.1 Correcting for the monochromator

Before using the set-up presented in Figure (11), the monochromator required correcting. It is difficult to physically re-align the monochromator, hence a relationship between the expected output wavelength and the true output wavelength needs to be established. The experimental set-up for correcting the monochromator is shown in Figure (12)

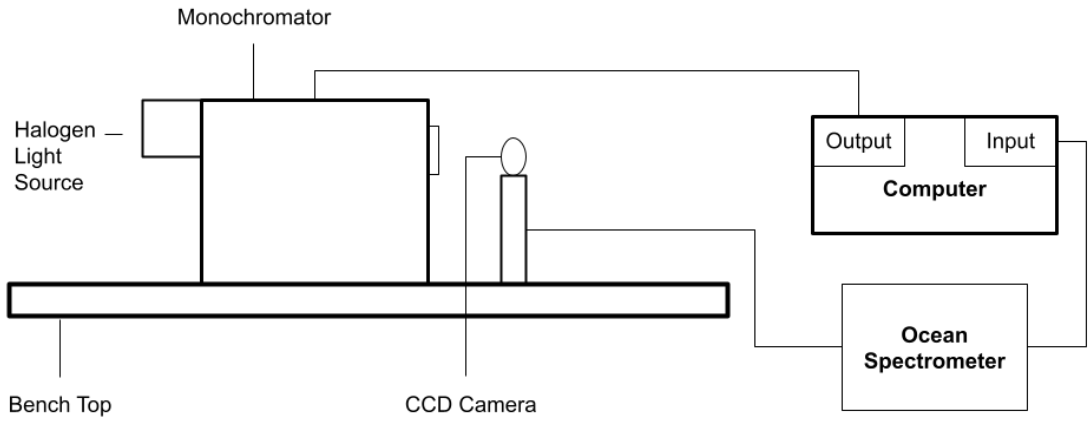

Figure 12: This Figure presents the experimental set-up used to correct the monochromator

where light from the monochromator is shone into a charge coupled device (CCD) camera. The CCD camera is connected to an Ocean Optics USB4000 spectrometer inputted to the computer. Data from the ocean spectrometer was analysed using Ocean Spectra Suite software. Note before correcting the monochromator using the CCD camera, the Ocean Optics spectrometer required calibrating. This was done using an Ocean Optics HG-1 mercury argon calibration source. Using Spectra Suite, emission lines from the mercury argon calibrator were compared to those output by the spectrometer. This gave an estimate on the error of the

spectrometer to be $\pm$1.6nm.

To correct the monochromator, the C file was used to manually output various wavelengths from the monochromator ranging between 400nm and 1000nm. This wavelength range was selected to align with the sensitivity range of the photodetector. Each wavelength value output by the C code to the monochromator in the range was compared to the emission peak produced by the spectrometer in Spectra Suite. In combination with the error on the spectrometer, a relationship between the wavelength input on the computer and the true wavelength emitted can be created.

3.2 The automated system

Once the monochromator is corrected, the equipment presented in Figure (11) can be used to form the automated optical absorption system. A video showing the operation of the system can be seen in the supplementary material, file A . The sample used to test the operation of the automated system was a double-sided polished crystalline GaAs wafer. The code process is presented in the flow diagram in Figure (13). The script firstly produces a user-friendly interface window in which parameters for operating the system can be input. These include start and end wavelength, number of readings per wavelength and wavelength step. Users then dictate which data analysis technique they desire to calculate the band gap. An image of the interface is presented in the supplementary material, file B. The user inputted parameters are then loaded into the Python script. The code will then set the stepper motor to the desired start wavelength and store the stepper motor counter and multimeter voltage data. Providing the stepper motor wavelength is less than or equal to the stop wavelength, the wavelength step is added to the stepping motor and this process loops until this condition is no longer met.

Once the loop has terminated, the data stored for each wavelength is saved into a file and imported back into MATLAB. First, the wavelength values for the monochromator need to be corrected using the relationship developed between the input wavelength and the emitted wavelength in Section (3.1). The voltages were then normalised to zero because when the sample is optically opaque, the voltage theoretically should be zero. However, there was some intrinsic noise within the circuit of the system. By normalising the lowest voltage recorded to zero and all other points accordingly, this noise is accounted for. From here, the data analysis differs depending on which method was prescribed by the user. These methods include the rapid method designed to be fully automated and quickest; the reputable Tauc method and the sigmoid-Boltzmann technique, a novel technique known for its simplicity.

3.2.1 Rapid method

The rapid method relies on a direct extrapolation of the linear region in the raw transmission data to determine the energy band gap. This first required determining which portion of the transmission data was considered to be linear. This was done by first considering the gradient between every adjacent data point in the whole data set. If these gradients were calculated to be above or below a certain gradient value, each point was assigned a true or false value respectively. This created a Boolean expression where only the true data points were selected to form the linear region. A straight-line of best fit was then fitted to the linear portion of the spectrum. The straight-line fit's coefficients were used to derive the horizontal axis intercept

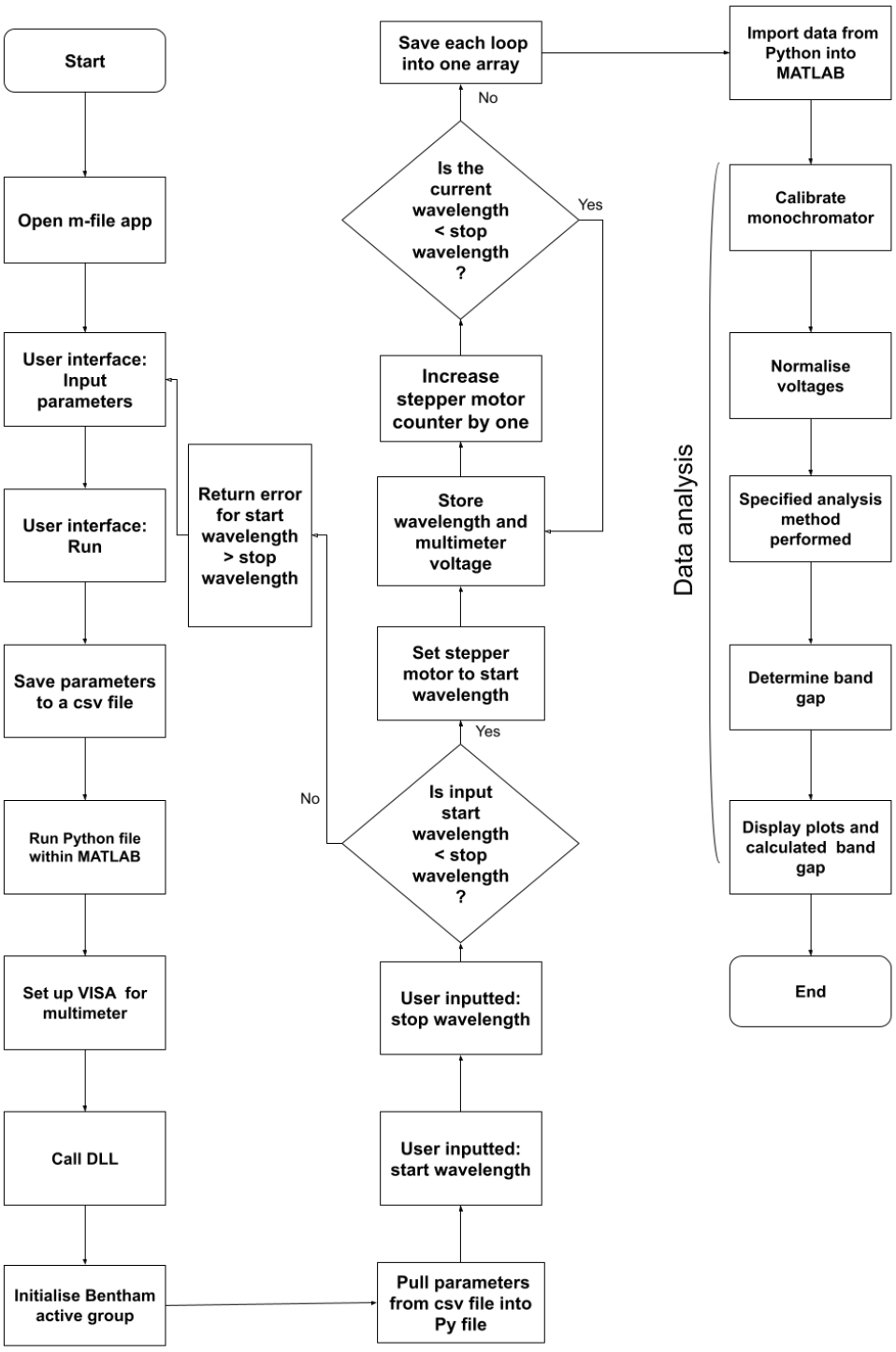

Figure 13: This Figure shows a flow diagram for the code of the automated system in full. Rectangles show a step within the automated process, curved rectangles represent the start or end of the process and diamonds show a logic step within the system

value which is equivalent to the energy band gap in this method. The plots desired by the user along with the calculated energy band gap are then displayed.

3.2.2 Tauc method

Next, the more traditional Tauc plot method was used to determine the band gap of the semiconductor. This utilised the same equipment set-up as shown in Figure (11), hence the system did not need re-calibrating. This method required calculating the absorption coefficient from the transmission coefficient. Since $T = \frac{I}{I_0}$, $\frac{I}{I_0} = \frac{V}{V_0}$ as photodetector voltage represents intensity, a baseline voltage reading without a sample was recorded. This reading was used for all calculations of transmission and absorption coefficients. Once the data had been corrected and normalised, the transmission coefficients were calculated alongside determining the reflectance value, R. The R value changes for each wavelength and for simplicity in experiments R is often estimated as a constant for the region of interest. However, to maximise the accuracy of this method, R was calculated for each wavelength via experimental data given by K.Papatryfonos *et al*[23]. Papatryfonos' data did not cover every wavelength in the range required, so a MATLAB file was generated to interpolate what the R value should be from the nearest data point to get the most accurate estimate. The last component to calculating the absorption coefficient is measuring the wafer thickness, t, which was measured to be (0.44$\pm$0.01) mm using a micrometre. Using parameters T, R and t, the absorption coefficients (α) could be calculated for the data set using Equation (34).

Unlike the rapid method, the Tauc method is dependent on whether the band gap of the material is direct or indirect. Consequently, once the run is complete the user is taken to a user interface window in which any of α, α^2 and $\alpha^{\frac{1}{2}}$ against energy can be plotted depending on the band gap type. This can be viewed in the supplementary material, file C. A straight-line of best fit is fitted to the linear portion of the selected plot. This straight-line can be refined within the app by changing the portion of the plot that is considered to be linear to best align with the appropriate portion of the experimental data. The corresponding straight-line fit's coefficients determine the horizontal intercept value and consequently the band gap of the material.

3.2.3 Sigmoid-Boltzmann method

The final data analysis method used to calculate the band gap was the sigmoid-Boltzmann function technique. Considering the profile of an absorption coefficient against energy plot (an s-shape within two horizontal asymptotes), it strongly resembles the shape of the Boltzmann function with some predictability. By mapping a Boltzmann function to an absorption coefficient against energy plot, the material's energy band gap can be calculated empirically from the parameters of the mapped function. Equation (35) presents the sigmoid function used to map the absorption coefficient plot

$$\alpha(E) = \alpha_{\text{max}} + \frac{\alpha_{\text{min}} - \alpha_{\text{max}}}{1 + \exp\left(\frac{E - E_0}{\delta E}\right)} \tag{35}$$

where α_{max} (α_{min}) stands for maximum (minimum) absorption coefficient, E_0 is the energy coordinate at which the absorption coefficient is halfway between its minimum and maximum value and δE describes the slope of the function. From this function the energy band gap can be calculated using the equation

$$E_g = E_0 - (\mathsf{n}_{\mathsf{dir/ind}} \times \delta E) \tag{36}$$

where $\mathsf{n}_{\mathsf{dir}} = 0.3$ and $\mathsf{n}_{\mathsf{ind}} = 4.3$, acting as correction factors depending on if the semiconductor has a direct or indirect band gap[24]. To automate the sigmoid-Boltzmann function analysis, first the absorption coefficients had to be attained. This was done in the same manner as the Tauc plotting method in Section (3.2.2). Having calculated the absorption coefficients, the α_{max} and α_{min} values were found, consequently determining E_0. These parameters were then entered into Equation (35) to provide the theoretically predicted shape of the absorption coefficient against energy plot. Parameter δE was altered with a slider within a MATLAB application to align the theoretical and experimental plots with each other. This can be seen in the supplementary material, file D. It should be noted that this technique will fail to produce an accurate band gap unless the theoretical fit reproduces a high proportion of the experimental fit. Next the appropriate parameters from Equation (35) could be used to calculate an estimate for the energy band gap using Equation (36).

4 Results

For proof of concept, a test sample of GaAs was used to display the operation of the automated system. However before operation, the monochromator required correcting.

4.1 Correction of the monochromator

The results for the monochromator correction are shown in Figure (14). The difference between the measured wavelength and the expected wavelength is plotted against the expected wavelength.

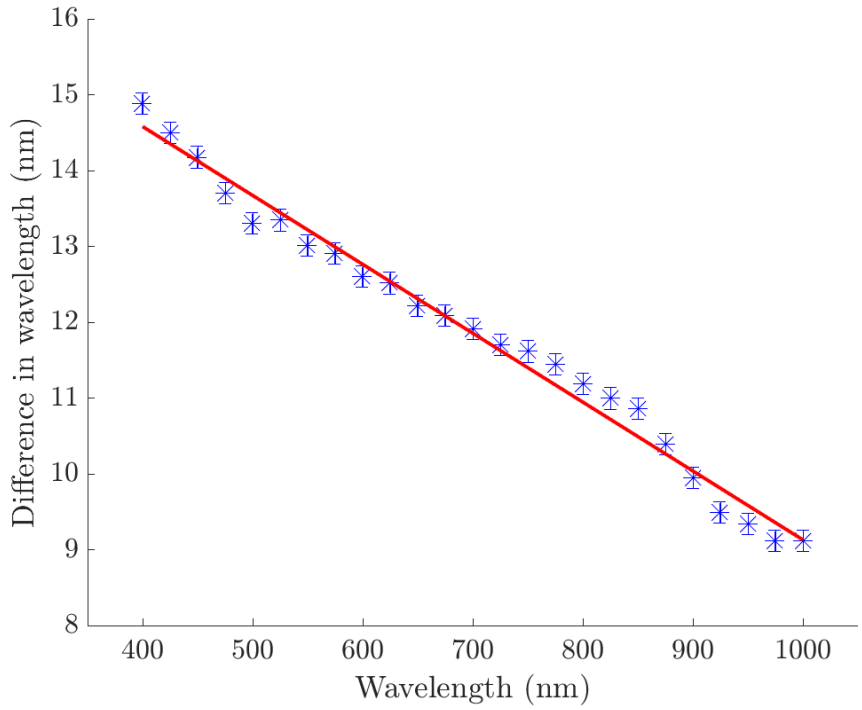

Figure 14: This Figure shows a plot of the wavelength difference between the measured wavelength and the expected wavelength, against the expected wavelength for the monochromator

A linear regression curve (red line) created using MATLAB's cftool was used to model the experimental data (blue markers). The regression has a gradient of -0.0091±0.0009 and a vertical intercept of (18.1±0.2)nm.

4.2 Optical absorption of GaAs

Now that the system has been corrected, a double-sided polished GaAs wafer was used as a test specimen for proof of concept.

4.2.1 Rapid Method

The automated system outputted the graph presented in Figure (15) for the rapid method.

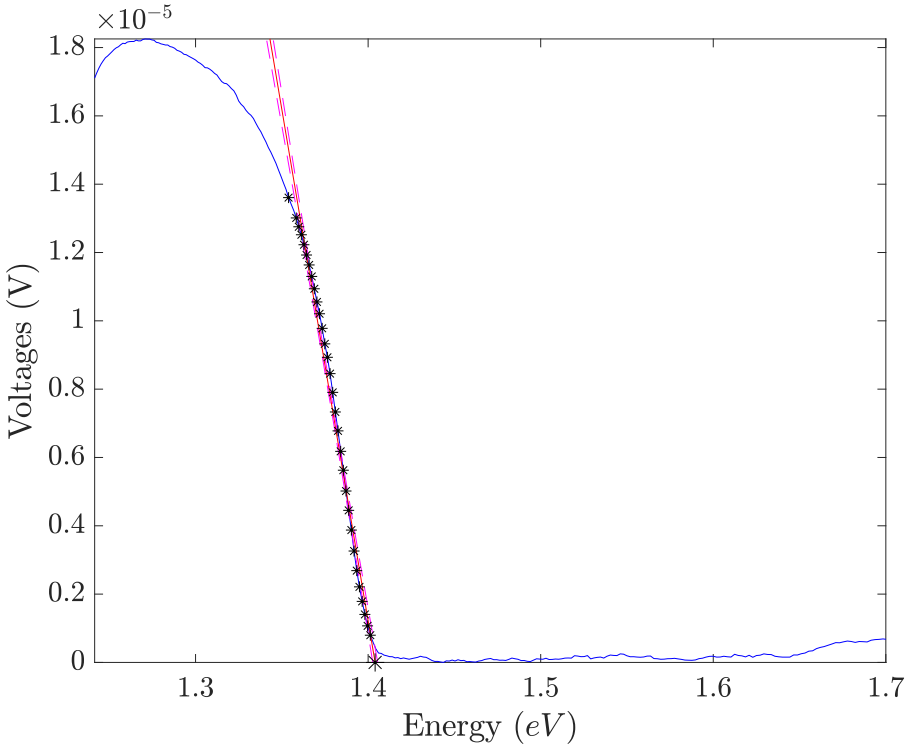

Figure 15: This Figure shows the final voltage against wavelength graph for the band gap calculation. The calculated band gap for this plot was (1.40 ± 0.05)eV

The blue plot of voltage against wavelength shows the full GaAs transmission spectrum. It should be noted that this spectrum is after data analysis. Hence, the monochromator has been accounted for and the voltages have been normalised to zero. The black asterisks indicate the portion of the spectrum that was considered to be linear. The red line shows the line of best fit for the linear portion of the spectrum with pink dashes outlining 95% confidence bounds. The black cross indicates the point at which the line of best fit intersects the horizontal axis. From the horizontal intersect, the band gap of the material can be determined. In this case, the band gap for GaAs was determined to be (1.40 ± 0.05)eV.

A graph showing the linear region of the voltage against wavelength plot in Figure (15) can be seen in Figure (16). All the points and lines are exactly the same as shown in Figure (15).

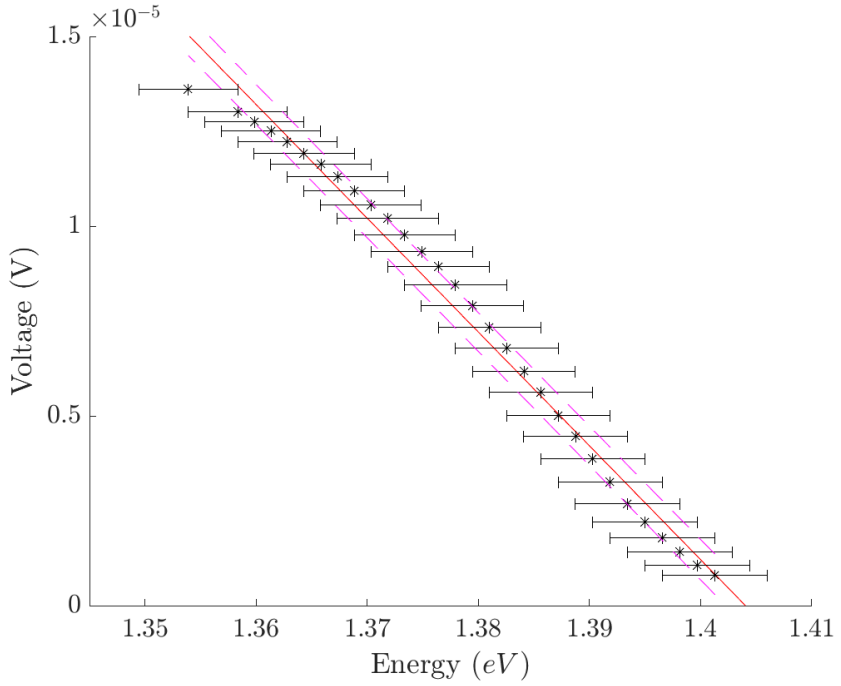

Figure 16: This Figure shows the linear portion of the transmission spectrum presented in Figure (15)

4.2.2 Tauc method

The second method that was used to calculate the band gap of the GaAs sample was the Tauc method. This method produced the graph shown in Figure (17

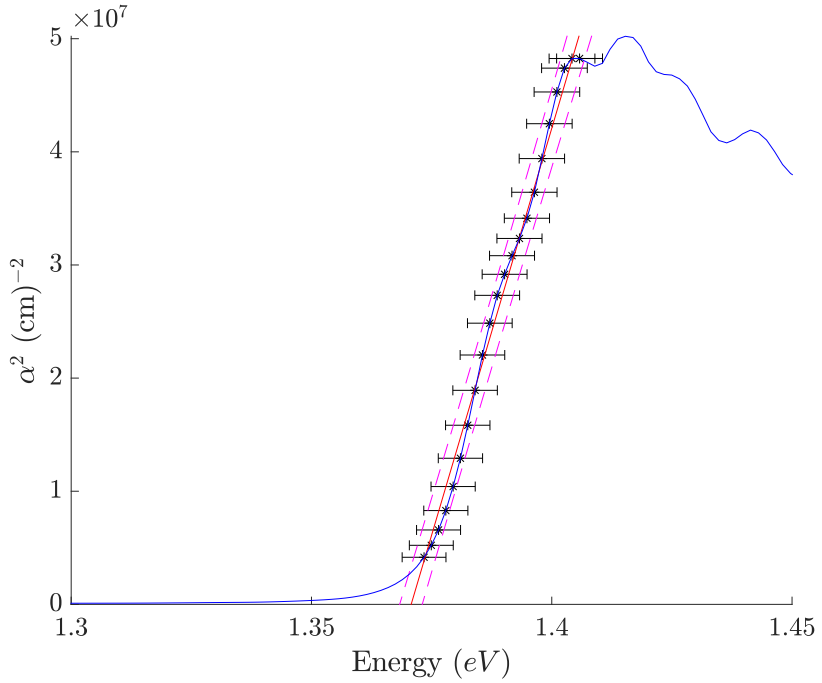

Figure 17: This Figure shows a plot of the absorption coefficient squared against energy for determining the bandgap of GaAs using the Tauc method

where the blue line represents the full transmission spectrum; the black asterisks show the selected linear region of the plot and the red line is the considered line of best fit for the linear region with pink dashes to show the 95% confidence bounds. The calculated band gap for this plot was (1.38 ± 0.05)eV.

4.2.3 Sigmoid-Boltzmann method

The final data analysis method used was the sigmoid-Boltzmann function technique. This involved fitting a theoretically determined function to an experimental absorption coefficient against energy plot. This can be seen in Figure (18) where the red line depicts the experimentally determined absorption coefficient against energy plot and the blue line is the sigmoid-Boltzmann function.

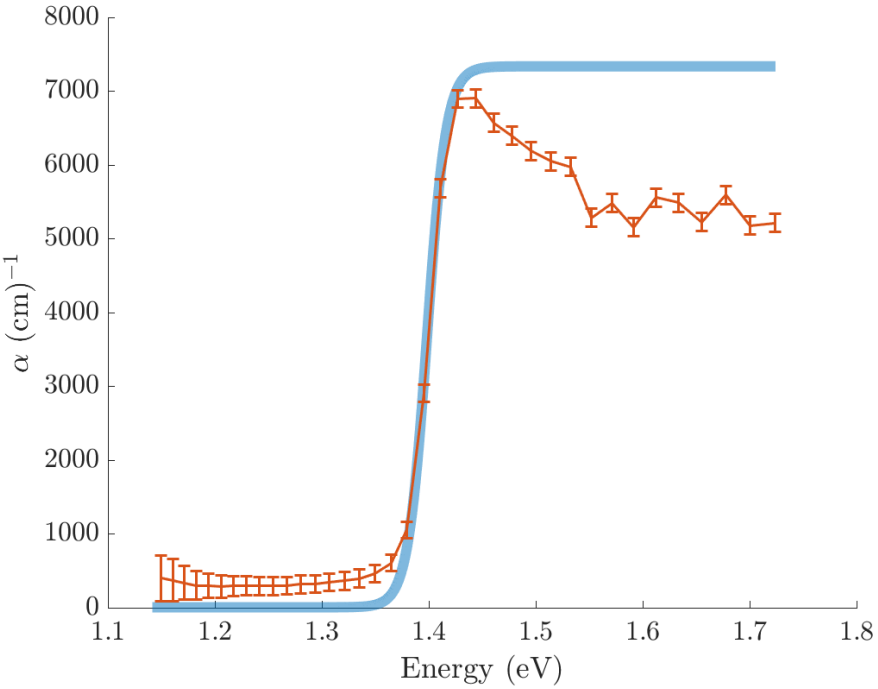

Figure 18: This Figure shows the experimentally determined absorption coefficient against energy plot (red). The blue function represents the accordingly mapped sigmoid-Boltzmann function

From this function, the band gap was calculated to be (1.40±0.01)eV.

For clarity, the energy band gaps calculated for GaAs using the three different methods are presented in Table (1).

Method	GaAs band gap (eV)
Rapid	1.40±0.05
Tauc	1.38±0.05
Sigmoid-Boltzmann	1.40±0.01

Table 1: This table presents the estimated GaAs band gaps from the three different methods used in this investigation

4.3 Error analysis

To combine errors one would typically use the error propagation equation

$$\sigma_f{}^2 = \sum_{i=1}^{N} \left(\frac{\partial f}{\partial x_i}\right)^2 \sigma x_i{}^2 \tag{37}$$

where σ_f is the error on the function being calculating, $\frac{\partial f}{\partial x_i}$ is the partial derivative of the function with respect to one of its variables and σx_i is the error on that associated variable. Equation (37) can be simplified to

$$\left(\frac{\sigma f}{f}\right)^2 = \sum_{i=1}^{N} \left(\frac{\sigma x_i}{x_i}\right)^2 \tag{38}$$

for trivial error propagation; however, it is less useful for complex functions. This was the case when calculating the error on the absorption coefficients. When calculating the error on Equation (34), Equation (37) was used. This rendered the partial derivatives

$$\frac{\partial \alpha}{\partial R} = \frac{R^2T^2\left(\frac{\frac{8RT^2-4(1-R)^3}{2\sqrt{4R^2T^2+(1-R)^4}}+2(1-R)}{2R^2T^2} - \frac{\sqrt{4R^2T^2+(1-R)^4}-(1-R)^2}{R^3T^2}\right)}{t(\sqrt{4R^2T^2+(1+R)^4}-(1-R)^2)} \tag{39}$$

$$\frac{\partial \alpha}{\partial T} = \frac{2R^2T^2\left(\frac{2}{T\sqrt{4R^2T^2+(1-R)^4}} - \frac{\sqrt{4R^2T^2+(1-R)^4}-(1-R)^2}{R^2T^3}\right)}{t(\sqrt{4R^2T^2+(1+R)^4}-(1-R)^2)} \tag{40}$$

$$\frac{\partial \alpha}{\partial t} = \frac{1}{t^2}\ln\left(\frac{((1-R)^4+4T^2R^2)^{0.5}-(1-R)^2}{2T^2R^2}\right) \tag{41}$$

Equations (39), (40) and (41) were substituted into Equation (37) to generate an error on the absorption coefficient using Equation (42).

$$\sigma_\alpha^2 = \left(\frac{\partial \alpha}{\partial R}\sigma_R\right)^2 + \left(\frac{\partial \alpha}{\partial T}\sigma_T\right)^2 + \left(\frac{\partial \alpha}{\partial t}\sigma_t\right)^2 \tag{42}$$

The same process was used to calculate the error on the sigmoid-Boltzmann band gap calculation presented in Equation (36). This generated partial derivatives:

$$\frac{\partial E_g}{\partial E_0} = 1 - (\mathsf{n}_{\mathsf{dir/ind}} \times \delta E) \tag{43}$$

$$\frac{\partial E_g}{\partial(\delta E)} = E_0 - \mathsf{n}_{\mathsf{dir/ind}} \tag{44}$$

Subbing Equations (43) and (44) into Equation (37), generates Equation (45)

$$\sigma_{E_g}^2 = \left(\frac{\partial E_g}{\partial(\delta E)}\sigma_{\delta E}\right)^2 + \left(\frac{\partial E_g}{\partial E_0}\sigma_{E_0}\right)^2 \tag{45}$$

which gives the error on the sigmoid-Boltzmann band gap. Other error calculations were done using the simple error propagation equation.

All the data in this experiment was analysed using MATLAB where cftool was used to fit an approximate function to most data sets. Cftool also provides the gradient and y intercept values along with their associated errors within 95% confidence bounds. To calculate the standard error on these coefficients, the confidence bounds B_{up} and B_{low} are used in Equation (46)

$$S = \frac{B_{up} - B_{low}}{2 \times 1.96} \tag{46}$$

where the factor 1.96 is introduced to reduce the confidence bounds to ∼68%.

5 Discussion of Results

5.1 Correcting the monochromator

The relationship between the expected wavelength and the true wavelength emitted by the monochromator was described by a straight-line of gradient -0.0091 ± 0.0009 and a vertical intercept of (18.1 ± 0.2)nm as shown in Figure (14). This plot includes the correction for the spectrometer. The error bars were estimated to be ±0.1nm due to the 2nm fluctuation on the emission peak in Spectra Suite.

The plot of the difference in wavelength against expected wavelength formed a clear negative linear correlation. A straight-line was fitted to this correlation using MATLAB's cftool. The error on the gradient and vertical intercept were calculated from MATLAB's 95% confidence bounds which were converted into a standard error using Equation (46). However, there is noticeable scatter around the straight-line fit which intersects only half of the error markers. This suggests that a random error was not accounted for in determining the error bars' magnitude. It could be said that the scatter around the fit in Figure (14) is somewhat sinusoidal. This small sinusoidal variation comes from the worm gear which powers the grating wheel within the monochromator. As the worm gear rotates, it does not advance the grating wheel at a uniform rate which gives rise to the oscillating pattern. This is expected within monochromators using a sine bar mechanism to control the rotation of the diffraction grating. However, the inconsistent period of the oscillation suggests the distribution is a combined random and sinusoidal error. This random contribution likely arises from the degradation of the sine bar mechanism. If out of alignment, the sine bar can cause inconsistent rotation of the diffraction grating. The random element in the distribution meant it was not possible to calibrate out the sinusoidal error and is likely the main contributor to the data scatter.

The negative linear regression in Figure (14) indicates a systematic error is produced within the monochromator. The origin of the difference in wavelength from the expected wavelength comes from the misalignment of the diffraction grating within the monochromator, meaning a different wavelength to the one expected is emitted from the exit slit. However, this difference in wavelength does not remain constant. A potential cause of the systematic decrease in wavelength could be from a variation in step size at which the diffraction grating is moving within the monochromator. At small wavelengths, the difference in wavelength between the true and expected wavelength is relatively larger than at large wavelengths. As the stepper motor rotates to larger wavelengths, each step incrementally does not rotate as much as the previous step. This causes a relatively smaller wavelength to be emitted from the exit slit than the previous wavelength, hence the difference in wavelength decreases for larger wavelengths. This is likely due to a mechanical fault within the monochromator where the stepper motor has lost its alignment.

5.2 Optical absorption of GaAs

A double sided polished GaAs wafer was used to test the functionality of the automated system for all three methods in this investigation.

5.2.1 Rapid method

In the rapid technique, the band gap of GaAs was determined to be (1.40 ± 0.05)eV from Figure (15). This is in agreement with the expected energy band gap of 1.42eV as this lies within the experimental value range. The band gap was calculated from the cftool coefficients (gradient and vertical intercept values) produced by the straight-line fit. The 95% confidence bound errors on the respective coefficients were converted to a standard error using Equation (46). The errors on the coefficients were combined using the simple error propagation equation (Equation (38)) to produce the error on the band gap. Error bars are omitted on this plot as they are too small to be visible.

A zoomed in plot of the linear region in Figure (15) is presented in Figure (16). This serves to provide a clearer depiction of the linear regression line that was fitted to the linear region of the plot. Error bars were derived from the 6nm bandwidth of the monochromator. The bandwidth in nanometres was converted to their equivalent bandwidth in electron volts for each data point. In this zoomed plot there is a noticeable undulation of data around the line of best fit. This arises from the nature of absorption in the semiconductor. The gradual increase in transmission stems from the photon energy approaching the absorption band edge, more commonly known as the Urbach tail, allowing a few electrons to not be absorbed. On the low energy end, deviation from the straight-line arises from the decrease in sensitivity of the Si photodetector at higher wavelengths causing a slump in voltage.

Nearly all of the data points lie within the 95% confidence bounds of the straight-line fit. This suggests that the confidence bound errors are consistent with the spread of the data. The error bars are likely an overestimation as the line of best fit comfortably intersects all error bars. As the error bars were derived from the monochromator's bandwidth, the error the bandwidth has contributed has been overcompensated. Although at the base of the monochromator's emission peak the bandwidth was 6nm, it still produced a definite peak where most of the emission took place at a bandwidth less than 3nm. Along with the error bars, it becomes

apparent in Figure (16) that the error on the energy band gap is also an overestimation. Although around the linear region shown the confidence bounds fit nicely around data spread, they are slowly diverging as energy decreases (voltage increases). If Figure (15) showed where the line of best fit intersected the vertical axis at 4.2×10^{-4} V, the confidence bounds would be significantly wider leading to a much larger error on the straight-line coefficients than is apparent in the portion of the spectrum this analysis is concerned with.

One error to consider is the extent of change on the line of best fit and the band gap if one more or less data point is considered in the straight-line region. From either end of the straight-line plot, by adding more data points the gradient will decrease and estimate the wavelength band gap as less (Urbach tail contributes more). However if points were removed from Figure (16) this would increase the gradient and increase the wavelength band gap estimation. This error was neglected because its magnitude was estimated to be less than 0.05eV. Note, this error might be more pertinent for an indirect semiconductor as the absorption edge is less sharp, meaning adding or removing one data point will have a bigger effect.

5.2.2 Tauc method

Next, the more traditional Tauc method was used to determine the band gap of the GaAs sample. The Tauc method estimated the bandgap to be (1.38$\pm$0.05)eV which is again consistent with the expected GaAs energy band gap. The band gap was calculated similarly to the rapid technique, despite the plots being different. By determining the horizontal intercept of the line of best fit in Figure (17) using the straight-line coefficients produced by cftool the band gap was ascertained. The 95% confidence bounds on the straight-line coefficients were converted into standard errors and propagated using Equation (38) to determine the error on the band gap. Again the error bars were derived from the 6nm bandwidth of the monochromator which has already been established as an overestimation in Section (5.2.1). The data spread is consistent with the 95% confidence bound range plotted where nearly all data points lie within this range. Likewise with the rapid method, the error on the band gap is likely an overestimation. For the same reasons as the rapid, the confidence bands begin to diverge as they approach the vertical axis, causing the error on the straight-line coefficients to be larger than anticipated from the region considered in Figure (17).

As the Tauc technique is only a semi-automatic process, the straight-line portion has to be selected manually by the user in a post analysis application app. This introduces ambiguity for what the user considers to be the linear portion of the spectrum. Even with this, for GaAs the range that feasibly could be argued as linear leads to a change in band gap of $\pm$0.004eV, significantly less than the current associated error.

Although the Tauc method has been well researched, it has been known to produce some erroneous estimates. When calculating the energy band gap of semiconductors with dense energy states beneath the conduction band, the Urbach tail can influence the Tauc plot and hence must be taken into account when calculating the band gap. In this case a direct application of the Tauc method results in an inaccurate estimation, often less than the expected band gap. This is because the spectrum of any non-pure semiconductor is a combination of the defects' and the semiconductor's absorption coefficients. To calculate the semiconductor's band gap accurately using Tauc analysis would require explicitly measuring the pure semiconductors absorption spectrum[25]. This could explain why the band gap calculation

underestimates the expected bandgap when using the Tauc method.

5.2.3 Sigmoid-Boltzmann method

The sigmoid-Boltzmann technique generated a GaAs band gap of (1.40±0.1) eV. This lies outside one standard deviation of the expected 1.42eV GaAs bandgap; this implies that the discrepancy in the calculated band gap and the expected band gap is less likely due to random error. The sigmoid plot was fitted using Equation (35) and reproduces a significant portion of the absorption spectrum. Although the horizontal asymptotes of the fit do not intersect a large quantity of the data, the slope region produces a near perfect alignment with the data which is the most important to ensure the reliability of this method. At higher energy values, a plateau appears in the plain absorption spectrum. This is likely not caused by the sensitivity of the photodetector as the absorption coefficients are calculated using a ratio of intensity (voltage) values. The cause of the downturn in absorption is due to the saturation of available energy states; since only a finite number of electrons can be promoted to the conduction band per Pauli's exclusion principle. The error bars were calculated from Equation (42) using the propagation described in Section (4.3). Errors on the absorption for the sigmoid-Boltzmann method are especially critical due to α determining the theoretical absorption spectrum. The error on the band gap was calculated using the error propagation that leads to Equation (45). The error on E_0 was derived from the errors on α_{max} and α_{min} to consider the range of possible α values at the midpoint between them. This was converted to a range of corresponding energy coordinates to give an error on E_0. Since the user is required to alter δE in a post analysis application, there is a range of sigmoid plots that could be reasoned as the best fit. Hence the error on δE was determined by finding the range of δE values for which the fit could within reason reproduce a large portion of the experimental data.

5.3 Method comparison

When comparing the methods, all have their advantages and disadvantages. In terms of automation, the rapid method is the clear favourite. Unlike with the Tauc and sigmoid-Boltzmann technique, the rapid method automatically produces an energy band gap without the user having to fine tune the model in a post analysis application. Despite this, the main benefit of the rapid method is that it does not require the thickness of the sample to be measured. If measuring multiple samples of varying thickness for the Tauc and sigmoid-Boltzmann techniques, the holistic process could become long negating any of the automation benefits. Another benefit of the rapid method is that it works independently of knowing whether the band gap is direct or indirect. However, this benefit is also its own demise. When comparing the rapid method to the less crude Tauc method, the Tauc analysis considers the band gap type meaning it can produce the appropriately scaled absorption spectrum in accordance with the theory. When fitting the straight-line this can help negate the influence the Urbach tail has on the band gap estimation. This is also the case with the sigmoid-Boltzmann technique, where the correction factor $n_{\text{dir/ind}}$ changes to account for the different band gap types.

The most precise method in the investigation is the sigmoid-Boltzmann. This is likely due to the Tauc and rapid method having to fit a straight-line to a curve. This always leads to subjectiveness as to what constitutes the linear portion and inevitably results in scatter about the best fit curve. The sigmoid-Boltzmann maps the absorption spectrum exactly and

calculates the band empirically from this model. Although there is ambiguity in aligning the sigmoid plot to the data, this isn't as significant as the Tauc method. It is difficult to argue which method is the most accurate as neither of the three exactly calculate the GaAs band gap to a high precision. However, it is clear that certain methods are beneficial over others under different circumstances. Measuring a number of semiconductors where only a crude band gap estimate is necessary would favour the rapid technique, yet for more precise readings one might favour the sigmoid-Boltzmann provided the transition type is known.

Although this investigation has successfully built an automated optical absorption system that can calculate a material's band gap to within a certain degree of uncertainty, there are still some clear flaws. The first is with the experimental set-up. The sensitivity range of the Si photodetector within the system is 300-1100nm. Hence if a user was measuring an unknown wide bandgap semiconductor outside of this range, no bandgap would be measured. To accommodate for this, the photodetector would need to be switched to one with an appropriate sensitivity range. This diminishes the universality of the system emphasised by the necessity to record another baseline voltage data set for the Tauc and sigmoid-Boltzmann methods for each photodetector used. Another issue is that two of three analysis methods are only partially automated. This means that the user has to help the system analyse the data for the Tauc and sigmoid-Boltzmann techniques. This again is time consuming and retracts from the holistic automation of the system. A next step would be to employ machine learning techniques to automatically determine which region of the Tauc plot is linear or align the theoretical sigmoid plot with experimental data. This was however beyond the scope of this investigation.

Despite this, all of the estimated GaAs band gaps still lie short of the expected GaAs band gap. This suggests something other than the data analysis is affecting the band gap calculation. The obvious reason to consider is the presence of the Urbach slope on the GaAs band structure. The GaAs Urbach tail is well established in literature to be $\sim$ 7 meV [16]. Assuming this value for the Urbach tail would take all GaAs band gaps except Tauc further from the expected GaAs band gap. This suggests that perhaps the Urbach tail is not the reason for the discrepancy between the expected and experimental band gaps; although it would not be prudent to say the Urbach slope does not affect the band gap at all. One error source mentioned prior is the band width produced by the monochromator. The emission peak on the monochromator was approximately 6nm determined by the diffraction grating in the monochromator. The bandwidth was reduced to a minimum by narrowing the exit slit width on the monochromator. However without reducing the emitted intensity to near zero, the bandwidth could not be reduced any further. The bandwidth is likely the primary reason for all the estimated band gaps lagging behind the expected GaAs band gap. This is because as the photon energies increase and approach the semiconductor's absorption edge, some electrons with energies greater than the emission peak will have a high enough energy to induce absorption.

6 Conclusion

This experiment successfully established an automated optical absorption system incorporating three unique data analysis techniques that could determine the energy band gap of a semiconductor within an uncertainty range. Using a GaAs wafer as a test specimen yielded the results (1.40$\pm$0.05)eV, (1.38$\pm$0.05)eV and (1.40$\pm$0.01)eV for the rapid, Tauc and sigmoid-Boltzmann plots respectively.

References

[1] G. Busch, "Early history of the physics and chemistry of semiconductors-from doubts to fact in a hundred years," *European Journal of Physics*, vol. 10, no. 4, pp. 254–264, oct 1989. [Online]. Available: https://doi.org/10.1088/0143-0807/10/4/002

[2] H. Davy, "Farther researches on the magnetic phaenomena produced by electricity; with some new experiments on the properties of electrified bodies in their relations to conducting powers and temperature," *Philosophical Transactions of the Royal Society of London*, vol. 111, pp. 425–439, 1821. [Online]. Available: http://www.jstor.org/stable/107627

[3] M. Faraday, "Experimental researches in electricity," *Philosophical Transactions of the Royal Society of London*, vol. 122, pp. 125–162, 1832. [Online]. Available: http://www.jstor.org/stable/107956

[4] H. Corporation., "History of semiconductors : Hitachi high-tech global," 2022. [Online]. Available: https://www.hitachi-hightech.com/global/products/device/semiconductor/history.html

[5] G. Malanowski, *The Race for Wireless: How Radio was Invented (or Discovered?)*. AuthorHouse, 2011. [Online]. Available: https://books.google.co.uk/books?id=IAjtEeVtXqAC

[6] T. Watkins, "History of the transistor." [Online]. Available: https://www2.sjsu.edu/faculty/watkins/transist.htm

[7] 2022. [Online]. Available: https://www.businessinsider.com/how-silicon-valley-got-its-name-2017-12?r=US&IR=T

[8] Z. Zu, "The 2022 sia factbook: Your source for semiconductor industry data," 2022. [Online]. Available: https://www.semiconductors.org/the-2022-sia-factbook-your-source-for-semiconductor-industry-data/

[9] "Semiconductor market size, by component, 2022-2029." [Online]. Available: https://www.fortunebusinessinsights.com/semiconductor-market-102365

[10] J. Singh, *Electronic and Optoelectronic Properties of Semiconductor Structures*. Cambridge University Press, 2003.

[11] D. Paschotta, "Band gap," 2022. [Online]. Available: https://www.rp-photonics.com/band_gap.html

[12] E. R. Johnson and S. M. Christian, "Some properties of germanium-silicon alloys," *Phys. Rev.*, vol. 95, pp. 560–561, Jul 1954. [Online]. Available: https://link.aps.org/doi/10.1103/PhysRev.95.560

[13] I. Mártil and G. G. Díaz, "Undergraduate laboratory experiment: Measurement of the complex refractive index and the band gap of a thin film semiconductor," *American Journal of Physics*, vol. 60, no. 1, pp. 83–86, 1992.

[14] L. Kirkup and F. Placido, "Undergraduate experiment: Determination of the band gap in germanium and silicon," *American Journal of Physics*, vol. 54, pp. 918–920, 1986.

[15] Y. Zhuo, A. Mansouri Tehrani, and J. Brgoch, "Predicting the band gaps of inorganic solids by machine learning," *The Journal of Physical Chemistry Letters*, vol. 9, no. 7, pp. 1668–1673, 2018, pMID: 29532658. [Online]. Available: https://doi.org/10.1021/acs.jpclett.8b00124

[16] J. I. Pankove and D. A. Kiewit, "Optical processes in semiconductors," *Journal of The Electrochemical Society*, vol. 119, no. 5, p. 156C, 1972. [Online]. Available: https://doi.org/10.1149/1.2404256

[17] D. Fraser, *The Physics of Semiconductor Devices*, ser. Oxford Science Publications. Clarendon Press, 1979. [Online]. Available: https://books.google.co.uk/books?id=Ze0WAQAAMAAJ

[18] J.-P. Leburton, "Optical absorption and luminescence," University of Illinois.

[19] F.-J. Haug, "Electrons in the band structure," Institute of Microtechnology, University of Neuchâtel.

[20] "Study of semiconductors by uv-vis spectroscopy," Belarusian State University and Department of Energy Physics.

[21] P. Y. U. K. Man, "Instrumental methods of analysis and laboratory," City University of Hong Kong.

[22] A. Hassanien and A. A. Akl, "Effect of se addition on optical and electrical properties of chalcogenide cdsse thin films," *Superlattices and Microstructures*, vol. 89, pp. 153–169, 2016. [Online]. Available: https://www.sciencedirect.com/science/article/pii/S0749603615302615

[23] K. Papatryfonos, T. Angelova, A. Brimont, B. Reid, S. Guldin, P. R. Smith, M. Tang, K. Li, A. J. Seeds, H. Liu, and D. R. Selviah, "Refractive indices of mbe-grown alxga(1-x)as ternary alloys in the transparent wavelength region," *AIP Advances*, vol. 11, no. 2, p. 025327, 2021. [Online]. Available: https://doi.org/10.1063/5.0039631

[24] A. R. Zanatta, "Revisiting the optical bandgap of semiconductors and the proposal of a unified methodology to its determination," *Scientific reports*, vol. 9, no. 1, pp. 11 225–11 225, Aug 2019, 31375719[pmid]. [Online]. Available: https://doi.org/10.1038/s41598-019-47670-y

[25] P. Makuła, M. Pacia, and W. Macyk, "How to correctly determine the band gap energy of modified semiconductor photocatalysts based on uv–vis spectra," *The Journal of Physical Chemistry Letters*, vol. 9, no. 23, pp. 6814–6817, 2018. [Online]. Available: https://doi.org/10.1021/acs.jpclett.8b02892